Self-Assembled CdSe/CdS Nanorod Sheets Studied in the Bulk Suspension by Magnetic Alignment

Francesca Pietra,[†,⊥] Freddy T. Rabouw,[†,⊥] Peter G. van Rhee,[‡] Jos van Rijssel,[§] Andrei V. Petukhov,[§] Ben H. Erné,[§] Peter C. M. Christianen,[‡] Celso de Mello Donegá,[†] and Daniël Vanmaekelbergh*[,†]

[†]Condensed Matter and Interfaces, Debye Institute for Nanomaterials Science, Princetonplein 1, 3584 CC Utrecht, The Netherlands, [‡]High Field Magnet Laboratory, Institute for Molecules and Materials, Radboud University Nijmegen, Toernooiveld 7, 6525 ED Nijmegen, The Netherlands, and [§]Physical and Colloid Chemistry, Debye Institute for Nanomaterials Science, Padualaan 8, 3584 CH Utrecht, The Netherlands. [⊥]F. Pietra and F.T. Rabouw have contributed equally to this work.

ABSTRACT We studied spontaneously self-assembled aggregates in a suspension of CdSe/CdS core/shell nanorods (NRs). The influence of the length and concentration of the NRs and the suspension temperature on the size of the aggregates was investigated using *in situ* small-angle X-ray scattering (SAXS) and linear dichroism (LD) measurements under high magnetic fields (up to 30 T). The SAXS patterns reveal the existence of crystalline 2-dimensional sheets of ordered NRs with an unusually large distance between the rods. The LD measurements show that the size of the sheets depends on the free-energy driving force for NR self-assembly. More precisely, the sheets are larger if the attraction between NRs is stronger, if the temperature is lower, or if the NR concentration is higher. We show that the formation of large NR sheets is a slow process that can take days. Our *in situ* results of the structures that spontaneously form in the bulk suspension could further our understanding of NR self-assembly into mono- or multilayer superlattices that occurs at the suspension/air interface upon evaporation of the solvent.

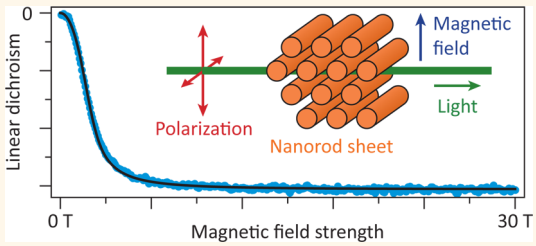

KEYWORDS: colloidal nanorod · magnetic linear dichroism · superlattice · small-angle X-ray scattering · self-assembly

Colloidal semiconductor nanocrystals (NCs) have attracted significant attention over the past decade as tailored building blocks for application in optoelectronic devices such as LEDs,[1−3] lasers,[4] and solar cells.[5−8] Moreover, self-assembly of NCs into ordered superstructures may lead to new types of materials, where properties are determined by the individual building blocks as well as by electronic coupling between them.[9] In this respect, formation of NC membranes at the liquid−air interface has emerged as a promising method to fabricate functional thin films.[10−17] In particular, nanorods (NRs) with a spherical CdSe core and a rod-shaped CdS shell have been shown to be chemically stable, have interesting optical properties,[18,19] and are able to form two-dimensional superstructures.[16,20−22]

Previously, we reported an *in situ* study of the self-assembly dynamics of such NRs at the liquid/air interface, using grazing incidence small-angle X-ray scattering (GISAXS).[16] Although the limited penetration depth (20 nm) of the X-ray beam into the solution prohibited direct visualization, our results suggested the formation of preordered NR sheets in the bulk dispersion as a potentially important factor for the NR ordering at the liquid/air interface. Similar mechanisms of preorganization were proposed in other works of NR self-assembly.[20−22] For example, Zanella et al.[20] found that NR superstructures could be grown equally well on a variety of substrates, suggesting that preorganization takes place in the bulk solution. However, until now these important preorganized NR structures have not been investigated in detail and their existence has only been proven indirectly.

In this work, we perform a direct *in situ* study of preorganized structures of CdSe/CdS NRs in bulk solution. Previously, only the organization of spherical NCs in bulk solution has been investigated, either using small-angle X-ray scattering (SAXS)[23] or cryo transmission electron microscopy (cryo-TEM).[24] The most important difference between spherical NCs and the NRs

* Address correspondence to d.vanmaekelbergh@uu.nl.

Received for review July 14, 2014 and accepted September 8, 2014.

Published online September 08, 2014
10.1021/nn503857t

that we study here is that NRs have strong side-to-side interactions. There are van der Waals attractions even when suspended in a good solvent, and there may be interactions mediated by the capping ligands and solvent molecules.[25] To investigate the resulting self-assembled superstructures we combine SAXS and magnetic-field induced linear dichroism (LD). The latter technique exploits the anisotropy of light absorption in elongated NRs: light polarized along the long axis is more strongly absorbed than light polarized perpendicularly.

The magnetic-field induced LD measurements yield information about the size of the preorganized NR sheets in the suspension, because only sufficiently large sheets are aligned by a magnetic field,[26−31] thus giving rise to a LD signal. Even at the highest magnetic field strengths of 30 T, the magnetic alignment energy of an individual CdSe/CdS NR, exhibiting only a weak diamagnetic response, is far below the thermal energy. Using this, we examine the distribution between individual NRs and NR aggregates as a function of various parameters: temperature, NR concentration, and NR length. Furthermore, we study the effect of the addition of a bad solvent which increases the van der Waals attractions.

RESULTS AND DISCUSSION

Three different NR batches were investigated: (i) long NRs with length L = (40 ± 4) nm and diameter $2R$ = (4.1 ± 0.4) nm, (ii) medium-length NRs with L = (23.1 ± 2.2) nm and $2R$ = (4.9 ± 1.1) nm, and (iii) short NRs with L = (16.1 ± 2.4) nm and $2R$ = (4.8 ± 0.4) nm (Supporting Information, Figure S1). The NRs were synthesized using a seeded-growth approach (see the Methods section for details),[32] where the growth of the rod-shaped shell occurs along the c-axis of the wurtzite CdSe seed nanocrystal.[33] The NRs are capped by octadecylphosphonic acid (ODPA). All experiments are done with the NRs dispersed in toluene.

Study of the NR Bundles in Solution by Small Angle X-ray Scattering. The SAXS study was performed at two temperatures, 26 and 60 °C, in order to observe the effect of the temperature on the formation of NR aggregates in suspension. We used suspensions with a volume fraction of 5.4×10^{-4} for the long, 4.5×10^{-4} for the medium-length, and 3.0×10^{-4} for the short NRs (such that molar concentrations are all 1.7 μM).

Figure 1 shows the SAXS patterns for short (Figure 1a,d), medium-length (Figure 1b,e), and long NRs (Figure 1c,f), recorded at 26 and 60 °C. Figure 1g−i shows the corresponding 1-dimensional scattering plots, obtained

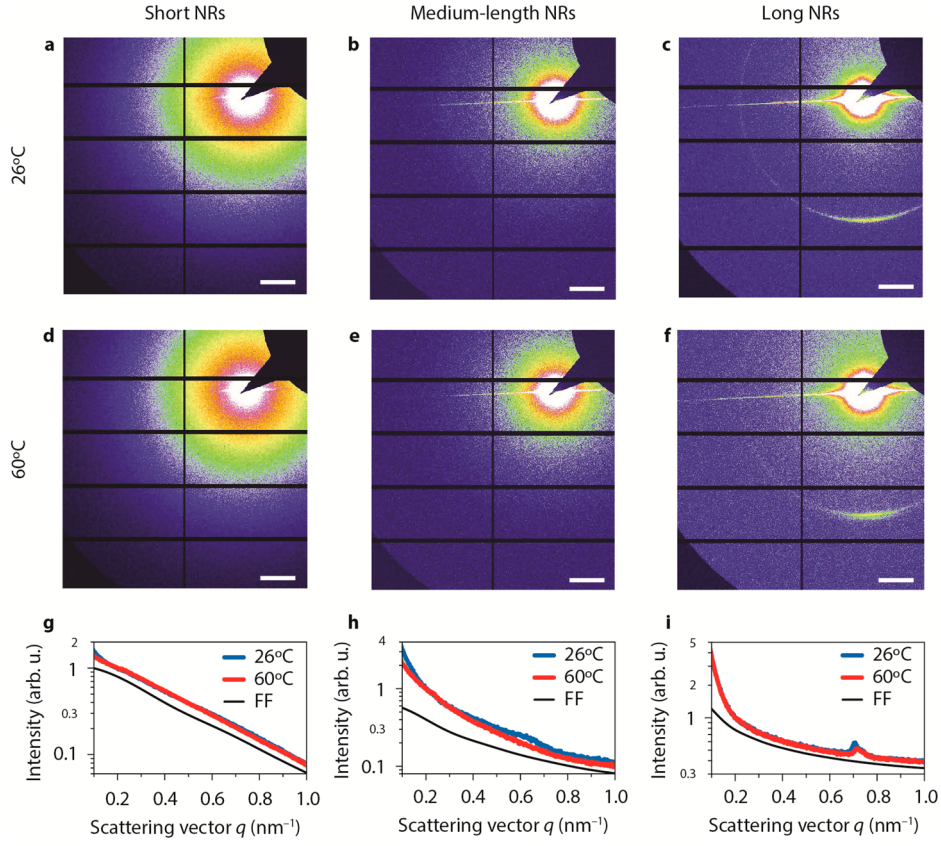

Figure 1. (a−c) SAXS patterns of suspensions of (a) short NRs, (b) medium-length NRs, and (c) long NRs in toluene recorded at 26 °C. (d−f) SAXS patterns of (d) short NRs, (e) medium-length NRs, and (f) long NRs in toluene recorded at 60 °C. Scale bars are 0.2 nm^{-1}. (g−i) One dimensional scattering plots for (g) short NRs, (h) medium-length NRs, and (i) long NRs obtained by azimuthal integration of the 2D patterns. Solid black lines are the calculated orientationally averaged form factors of the NRs.

by integrating the 2-dimensional patterns as well as the theoretical form factors of the NRs.[34] In the case of short NRs (Figure 1a,d), the SAXS patterns at both temperatures are dominated by the form factor; no clear structure factor features are observable. This shows that short NRs do not form aggregates or that the aggregates are too small to induce any observable diffraction. Figure 1b, e shows the SAXS patterns for medium-length NRs. Similarly, the patterns are dominated by the form factor and no clear structure factor is observable. The 1-dimensional scattering plot (Figure 1h) at 26 °C, however, shows that there is a weak broad peak around q = 0.65 nm^{-1} corresponding to a lattice spacing of roughly $d = 2\pi/q$ = 9.6 nm. Higher order diffraction peaks are not visible. The peak disappears upon increasing the temperature to 60 °C, indicative for the dissociation of the bundles. Figure 1c,f shows the SAXS patterns of the sample of long NRs recorded at 26 and 60 °C. We note that the SAXS pattern is anisotropic, indicating that the orientation of the sheets is not entirely random (something we do not observe with LD in the absence of a magnetic field; see below). The anisotropy might be due to spatial confinement of the sheets in the small SAXS capillary (500 μm diameter) and/or slow sedimentation. The pattern at 26 °C has a diffraction ring of radius q = 0.70 nm^{-1}, corresponding to a lattice spacing of d = 9.0 nm. In contrast to the case of medium-length NRs, a clear diffraction peak can still be observed at higher temperature (60 °C). Furthermore, if we compare the SAXS patterns of medium-length to the ones of long NRs, it is clear that medium-length NRs show a lower scattering intensity. We thus conclude that, compared to the medium-length NRs, the long ones form larger bundles which are less susceptible to dissociation at elevated temperatures.

A second point to note is that the observed lattice spacings (of a NR diameter plus more than 4 nm) are larger than one would expect for NRs assembled side-to-side in a close-packed fashion, separated only by the length of the ligands. Apparently the NRs form a loose structure in the bulk suspension, with the region between adjacent NRs partially filled with solvent molecules. This may also explain why we do not observe higher-order peaks in the SAXS patterns (Figure 1g–i), as the NRs are probably rather loosely fixed to their exact lattice positions leading to a strong Debye–Waller effect diminishing the visibility of higher-order reflections.[35] In contrast, we have previously observed that once NRs adsorb on the liquid/air interface, the interparticle separation (2.5–3.5 nm) is smaller[16] and probably set only by the ligand capping layers. We conclude that on the liquid/air interface capillary forces pull NRs closer together than they are in the bulk suspension. As a side note, we also found previously[16] that drying of a NR superstructure formed at the liquid/air interface causes additional contraction (to 1.2–2.5 nm separation) as, presumably, the ligand layers interdigitate.

The SAXS patterns indicate that the bundles, in fact, constitute sheets of a monolayer of NRs, organized side-to-side. Stacking of such sheets would result in a peak at low q values around 0.15–0.3 nm^{-1}, i.e., at $2\pi/L$, with the interlayer distance L roughly equal to the NR length. Since this peak is absent in Figure 1g–i, we conclude that the sheets are mostly monolayers. For the long NRs, we can estimate the grain size to be $D = 2\pi/\Delta q$ = 360 nm, where Δq is the full-width-at-half-maximum (fwhm) of the structure factor peak. This corresponds to approximately 1600 NRs per crystalline domain. In view of results reported below, we should however realize that the sheets in the suspension may actually have (much) larger lateral dimensions and must thus consist of several crystalline domains separated by grain boundaries.

Study of the Orientation of the NR Bundles in a Magnetic Field by Optical LD. In a second set of experiments, we aimed to investigate how the mean size of NR sheets in suspension depends on NR length, temperature, NR concentration, and the addition of nonsolvent. The experimental setup is schematically depicted in Figure 2 (see the Methods section for details). A 5 mm quartz cuvette containing a suspension of NRs in toluene was loaded in a resistive 33 T Florida-Bitter magnet, which can produce static magnetic fields with variable strength up to 33 T. The magnetic field is oriented vertically, in the z-direction. A phase modulated linearly (y and z) polarized light beam[36] passes

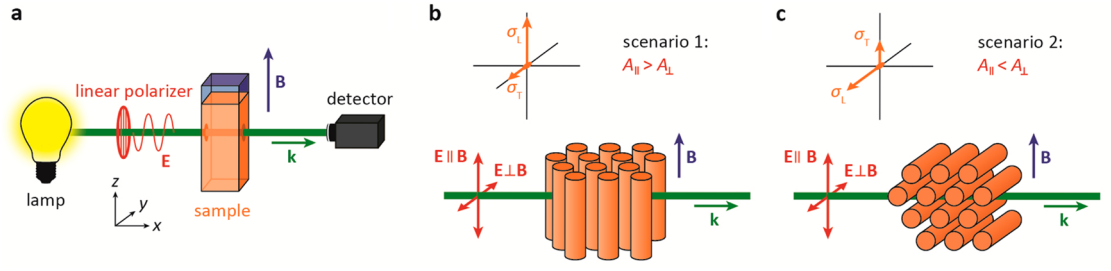

Figure 2. (a) Schematic of the experimental setup. We measure the transmission of polarized light through a sample of NRs, with the aligning magnetic field B perpendicular to the propagation direction of light k. (b) Scenario 1: if the NRs align with their long axis along B, then the absorption is stronger for light polarized along B than for light polarized perpendicularly ($A_{\parallel} > A_{\perp}$). (c) Scenario 2: if the NRs align with their short axis along B, then the situation is reversed ($A_{\parallel} < A_{\perp}$). σ_L and σ_T indicate the longitudinal and the transverse absorption cross-section, respectively.

through the sample horizontally, in the positive *x*-direction. Measurements are performed at the wavelength for which the optical density (OD) of the sample is equal to 1 at the default concentration of 1.7 μM (corresponding to volume fractions of 5.4×10^{-4} for the long, 4.5×10^{-4} for the medium-length, and 3.0×10^{-4} for the short NRs) at zero field, which corresponds to 475 nm for the long NRs, 480 nm for medium-length NRs, and 485 nm for the small NRs. The absorption of semiconductor NRs in the blue/UV spectral region is anisotropic due to depolarization effects: light polarized along the long NR axis is absorbed more strongly than light polarized perpendicularly[37] (see the Supporting Information for details). For an ensemble of randomly oriented NRs, the linear dichroism is zero, i.e., absorption of light for the two perpendicular polarization directions is equal. However, if the NRs align in the magnetic field, the degree of alignment can be quantified from the linear dichroism signal. This method has previously been used to determine the structures of organic molecules and other inorganic particles.[29,31]

To allow the results presented below to be properly appreciated, we first discuss the essentials of the method: (i) alignment of 2-dimensional sheets of NRs in the magnetic field and (ii) the absorption of nonresonant linearly polarized light in 2-dimensional NR sheets with a preferential orientation.

Alignment of 2-D NR Sheets in a Magnetic Field. Both the CdSe/CdS NRs and the solvent toluene are diamagnetic, with bulk volume susceptibilities χ of -2.1×10^{-5} (for CdS) and -7.8×10^{-6}, respectively.[38] These result in a magnetizability α^M of a single NR, defined by $\mathbf{m} = \alpha^M \mathbf{B}$ (where $\mathbf{m}$ is the magnetic dipole moment that is induced by a magnetic field $\mathbf{B}$). Because of demagnetization effects, the magnetizability of a NR is more negative in the transverse direction $\alpha_\perp^M$ than in the longitudinal direction $\alpha_\parallel^M$ (see the Supporting Information for details). As a result, the magnetic energy $E^M = -\mathbf{m} \cdot \mathbf{B}/2$ depends on the orientation of the NR with respect to the magnetic field. The orientation dependent part of the magnetic energy is

$$E^M = -\frac{1}{2}\Delta\alpha^M B^2 \cos^2\theta \qquad (1)$$

with $\Delta\alpha^M = \alpha_\parallel^M - \alpha_\perp^M > 0$ the anisotropy of the magnetizability, and θ the angle between the long NR axis and the magnetic field. E^M is minimum at $\theta = 0$, meaning that the preferential orientation of a single NR is along the magnetic field. However, the alignment energy is of the order of 10^{-8}–10^{-10}eV/NR even for magnetic fields up to 30 T, insufficient to overcome the thermal energy. It is therefore not possible to align individual NRs in a magnetic field.

The situation is, however, different for self-assembled sheets of NRs, where two important effects have to be taken into account. First, because of magnetic moments induced on neighboring NRs, the local magnetic field strength experienced by each NR is different from the externally applied magnetic field. This effect can be described using an "effective magnetizability" $\tilde{\alpha}^M$. The interaction between adjacent magnetic dipoles is such that magnetizability is enhanced for **B** directed along the short NR axis (corresponding to the long axis of the NR sheet) and reduced for the other direction (see the Supporting Information for details). As a result, the anisotropy $\Delta\alpha^M > 0$ is positive for a single NR, but the *effective* anisotropy $\Delta\tilde{\alpha}^M < 0$ for a NR incorporated in a 2-dimensional sheet is negative. In other words, while for individual NR the lowest-energy orientation is along the magnetic field, collective effects make that self-assembled NRs orient perpendicularly (note, however, that the sheet as a whole is then aligned along the field). Our experiments show that NR sheets indeed show this collective behavior: the NR bundles behave like scenario 2 in Figure 2c rather than scenario 1 in Figure 2b. The second collective effect is that the total magnetic alignment energy of the sheet is the sum of contributions from constituent NRs:

$$E^M = -N\frac{1}{2}\Delta\tilde{\alpha}^M B^2 \cos^2\theta \qquad (2)$$

where $\Delta\tilde{\alpha}^M = \tilde{\alpha}_\parallel^M - \tilde{\alpha}_\perp^M < 0$ is the anisotropy in the effective magnetizability and N is the number of NRs in the sheet. For sufficiently large N, the magnetic alignment energy can be high enough to overcome thermal randomization. Hence, only sufficiently large sheets can be aligned in a magnetic field. For our analysis we assume that the magnetic response of the NRs stems entirely from the semiconductor material, i.e., the contribution from the organic capping layer is assumed to be negligible. We further assume that the magnetic susceptibility of nanocrystalline CdS is identical to that of bulk CdS and isotropic. The anisotropy in the effective magnetizability then originates only from the spatial arrangement of semiconductor material, i.e., elongated rods ordered in a disk-shaped superstructure.

Anisotropic Absorption by Aligned NRs: The LD Signal. The linear dichroism (LD) signal is defined as the difference in absorbance A (= $-\log T$, with T the fraction of light transmitted) between light polarized along (*z*-polarized) and perpendicular to (*y*-polarized) the static magnetic field (see Figure 2):

$$\Delta A = A_\parallel - A_\perp \qquad (3)$$

The absorption cross-section σ of a NR depends on its orientation with respect to the polarization of the light. Absorption is maximal (σ_L) if the long axis is along the polarization direction and minimal (σ_T) if it is oriented perpendicularly. In the case of a NR orientation given by the polar angle θ and azimuthal angle φ, the absorption cross sections for the two polarizations are

$$\sigma_\parallel(\theta) = (\sigma_L - \sigma_T)\cos^2\theta + \sigma_T \qquad (4a)$$

$$\sigma_\perp(\theta, \varphi) = (\sigma_L - \sigma_T)\sin^2\theta \sin^2\varphi + \sigma_T \qquad (4b)$$

where ∥ and ⊥ denote light polarization along (*z*) and perpendicular (*y*) to the magnetic field. Under the influence of a magnetic field along *z*, the NR orientations can be described by normalized orientation distribution $p(\theta)$ of the polar angle (while the orientation in the *xy*-plane remains random). This yields for the LD signal of an ensemble of NRs

$$\Delta A = \rho l \int_0^{\pi} p(\theta) \frac{1}{2} (\sigma_L - \sigma_T)(3\cos^2\theta - 1) \sin\theta \, d\theta \quad (5)$$

where ρ and l are the NR concentration (number density) and the optical path length (5 mm), respectively. As expected, $\Delta A = 0$ for a fully random orientation distribution. The LD signal is $\rho l(\sigma_L - \sigma_T)$ in the case of full alignment of the NRs along the magnetic field (i.e., in the *z*-direction), or $\rho l(\sigma_T - \sigma_L)/2$ in the case of full alignment perpendicular to the magnetic field (i.e., in the *xy*-plane).

Since we use light with energy well above the bandgap of the NRs, the anisotropic absorption cross-section can be calculated from the bulk dielectric constant of CdS, using depolarization factors and approximating the NR shape as ellipsoidal.[37] For all three NR batches, $\sigma_L > \sigma_T$ (see the Supporting Information for details). Hence, the sign of the LD-signal is a direct indicator for the prefential a direction of the NRs. In all experiments we find $\Delta A \leq 0$, meaning that the NRs are preferentially oriented with the long axis perpendicular to the magnetic field.

The Equilibrium between Individual NRs and Sheets. NRs experience mutual attraction due to a combination of van der Waals interactions, dipolar interactions, and attraction forces mediated by the ligand layers and solvent molecules.[23] The equilibrium between individual NRs and sheets of size *N* can be written as

$$N \ \mathrm{NR} \leftrightarrow (\mathrm{NR})_N \quad (6)$$

At equilibrium the chemical potentials of the monomers $N\mu_1$ and of the *N*-mers μ_N are equal.[39] The chemical potentials depend on the volume fraction as $\mu_i = \mu_i^0 + k_BT \ln x_i$, where μ_i^0 is the refence chemical potential (at $x_i = 1$), k_BT is the thermal energy, and x_i is the volume fraction of *i*-mers. Solving for the equilibrium condition of equal chemical potentials for all species, one arrives at $x_N = x_1^N \exp[-(\mu_N^0 - N\mu_1^0)/k_BT]$. Considering only pair interactions, with energy minimum *u*, yields for volume fraction of sheets of size *N*

$$x_N = x_1^N \exp(-c_N u/k_BT) \quad (7)$$

where c_N is the number of NR-NR bonds in a sheet of size *N*. In large sheets with NRs close-packed side-to-side, the number of bonds $c_N \approx 3N$ (while in smaller sheets this number is somewhat lower because of NRs with low coordination on the edge of the sheet). Hence, we can distinguish two scenarios: (I) At low NR concentration or in case of weak NR−NR attraction ($x_1 \exp(-3u/k_BT) < 1$) the concentration of sheets x_N decreases exponentially with *N*. There is a "chemical" equilibrium between individual NRs and sheets containing up to a few tens of NRs. Our LD-measurements are insensitive to these small sheets, as their magnetic alignment energy eq 2 is too small: at most $10^{-6}k_BT$ for sheets of fewer than 100 NRs. (II) At high NR concentration or in the case of strong NR−NR attraction ($x_1 \exp(-3u/k_BT) > 1$) the concentration of sheets x_N diverges with increasing size *N*. The NRs undergo a "phase transition", ultimately to a single extremely large sheet. However, thermal and mechanical disruptions may result in the formation of many large but distinct sheets. In our LD experiments we only observe signal from these larger sheets.

We present our data as the LD-signal normalized by the total absorbance measured in the absence of a magnetic field. To model our data, we use eq 5 and assume monodisperse sheets containing *N* NRs, which have a Boltzmann orientation distribution $p(\theta) \propto \exp[-E^M(\theta)/kT]$ by magnetic alignment (eq 2). Supporting Figure S3 in the Supporting Information shows that the assumption of monodisperse sheets of size *N* or a wide Gaussian distribution around mean *N* yields very similar LD-signals. From a fit of the data to eq 5 we obtain the (mean) sheet size and the fraction of NRs organized in sheets sufficiently large to align in the magnetic field. In simple terms, the sheet size is determined from the magnetic field strength at which the LD-signal saturates and the fraction of NRs organized in large sheets from the magnitude of the LD-signal at saturation.

Effect of NR Length on Bundle Size. Figure 3 shows the LD-signal at room temperature as a function of applied magnetic field, for the three different NR lengths investigated. For all samples the signal is zero at zero-field. This proves that in the absence of a magnetic field the NRs are not macroscopically oriented (i.e., they are aligned in 2-dimensional sheets which as

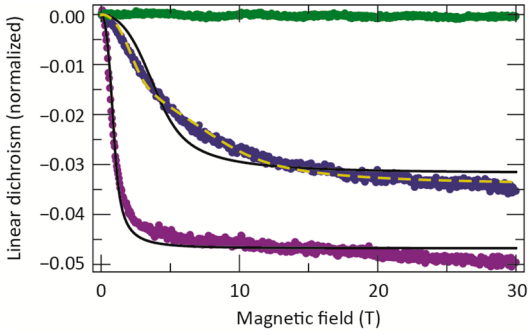

Figure 3. Linear dichroism of samples of short NRs (green), medium-length NRs (blue), and long NRs (purple) as a function of the applied magnetic field strength, measured at 20 °C. The signal is normalized to the nonpolarized absorbance. Solid black lines are fits to eq 5. Assuming a bimodal sheet size (yellow dashed line) leads to a better fit for the medium-length NR sample.

a whole, however, are not oriented). With increasing field strength a negative LD-signal builds up for the medium-length and long NRs, while nothing is visible for the short NRs. This indicates that only the medium-length and long NRs are assembled into bundles that are sufficiently large to be aligned by the magnetic field. From the sign of the LD-signal (see the theory section above), we conclude that the NR bundles are oriented such that the long axes of the NRs are perpendicular to the field, as in scenario 2 of Figure 2c. We fit the experimental data to eq 5 assuming a single population of NR bundles, and obtain $N\Delta\tilde{\alpha}^{M}/2k_BT$ = 4.2 T^{-2} and 0.21 T^{-2} for the long and for the medium-length NRs, respectively. These values correspond to 2.2 $\times$ 10^9 NRs/bundle for the case of long NRs and 1.9 $\times$ 10^8 NRs/bundle for the case of medium-length NRs. From the fit we also estimate that 21% and 15% of the NRs, respectively, are assembled into such large bundles. The remaining NRs are either assembled in bundles too small to become aligned or dispersed as individual NRs. We ascribe the deviation between experiment and fit in Figure 3 to our assumption of a monodisperse bundle size. Indeed, assuming a bimodal size distribution (yellow dashed line) leads to a better fit (see also Supporting Figure S3 in the Supporting Information), with a weighted average size of 3.1 $\times$ 10^8 NRs/bundle.

The numbers we estimate for the bundle sizes appear high, as they imply that the size of a NR sheets can be of the order of 100 μm. As a comparison, monolayer NR sheets grown at the liquid/air interface can be larger than 10 μm when imaged with TEM (see the Supporting Information Figure S2). These may even be mere fragments of the sheets that exist at the liquid/air interface but break when scooped on the TEM grid and dried in vacuum. We must however emphasize that the absolute values of size that we estimate from the magnetic-field induced LD measurements depend on the magnitude of the magnetic response that we use in our model (see the Supporting Information for details). This is subject to several uncertainties, such as the unknown but possibly large effect of nanoscale confinement on the magnetic susceptibility. Moreover, there may be a magnetic response from the ligands attached on the NR surface or from the chemical bond between core and ligand.[40] Fortunately, these uncertainties do not prohibit analysis of the effect of experimental parameters on the bundle sizes, although the estimates of the *absolute* sizes could be off.

The occurrence of a fraction of NRs assembled in large bundles, while the rest are individuals or are present in much smaller bundles, indicates that we are not in a situation of full thermodynamic equilibrium. We have a case of $x_1 \exp(-3u/k_BT) > 1$ (see the theory section above), i.e., we are closer to a phase transition than a chemical equilibrium. The thermodynamically most favorable ordering of the NRs would be one huge bundle that incorporates all NRs. On the basis of this, we can give upper bounds of the pair interaction strength u. The long NRs (total volume fraction $x = 5.4 \times 10^{-4}$) must have a pair interaction of at least $|u| > 2.5k_BT$, for the medium-length NRs ($x = 4.5 \times 10^{-4}$) the interaction strength must be at least $|u| > 2.6k_BT$, while between the short NRs ($x = 3.0 \times 10^{-4}$), which do not form extended sheets, the interaction is weaker than $|u| < 2.7k_BT$. There can be several contributions to the inter-NR interaction. From the SAXS measurements (Figure 1) we know that the equilibrium separation between the NRs is approximately 4 nm. We can estimate the contribution of van der Waals attraction between NRs at this separation (see the Supporting Information for details) to be $1.7k_BT$, $1.2k_BT$, and $0.8k_BT$ for long, medium-length, and short NRs, respectively. Hence, there must be an additional attractive contribution to account for the formation of extended sheets of long and medium-length NRs. Indeed, a recent theoretical study has revealed that ordering of ligand and solvent layers can result in an effective attractive inter-NR potential with minima deeper than expected from van der Waals attraction alone and at relatively large distances of $\sim$4 nm.[25] Hence, the combination of van der Waals interaction and ligand-mediated interactions can account for the formation of sheets. We estimate that possible contributions of magnetic-field induced dipolar interactions are negligible (weaker than 10^{-7} k_BT; see the Supporting Information). Furthermore, important contributions of repulsive electrostatic interactions can be excluded because (although they could be several k_BT strong) semiconductor nanocrystals are predominantly uncharged when dispersed in apolar solvents.[41] Finally, we note that excluded volume interactions at our relatively low NR concentrations are too weak to make a stable nematic liquid crystal phase of NR sheets in the absence of a magnetic field.[42]

This situation is different from the formation of spherical micelles from amphiphilic molecules, where steric effects lead to a finite optimum size. In the case of our NRs, the formation of one "supersheet" is made impossible by very slow kinetics for merging of separately nucleated sheets and the mechanical fragility of 2-dimensional sheets once they have grown large. There is an analogy with the precipitation of (3-dimensional) salt crystals from an oversaturated solution, which (unless nucleation proceeds slowly and in a controlled way) may lead to a few large crystal domains, while most others are small.

Next we examined, for the sample of long NRs, how we can influence the aggregation into large bundles. Figure 4a shows the LD-signal as a function of magnetic field for different parameters. The yellow curve is the same as displayed in Figure 3, for the default NR concentration of 1.7 μM. The red and green curves are obtained at 2$\times$ lower and 2$\times$ higher concentration,

respectively. The blue curve is obtained at the default NR concentration but with the addition of 20% (volume) of the bad solvent butanol. Solid black lines are fits to a single population of bundles (eq 5).

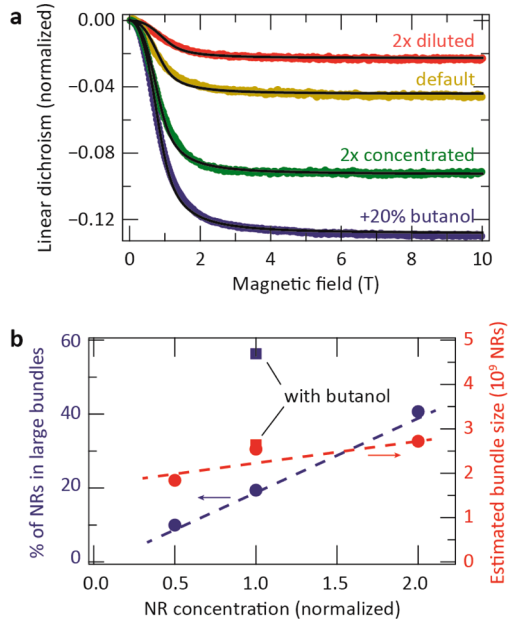

Figure 4. (a) Magnetic-field induced linear dichroism of the sample of long NRs, at the default concentration of 1.7 μM (corresponding to a volume fraction of 5.4×10^{-4}) in toluene (yellow), at 2× lower concentration (red), at 2× higher concentration (green), and after addition of 20% butanol. Solid black lines are fits to eq 5. (b) Fit results show that the fraction of NRs in large bundles (blue symbols) as well as the estimated bundle size (red symbols) increases with increasing NR concentration or with the addition of butanol (squares).

Figure 4b summarizes the fit results: the fraction of NRs in large bundles (blue) and the bundle size (red). Circles represent the samples with different NR concentration in pure toluene, while squares represent the sample with 20% butanol. We see that a higher overall NR concentration or the addition of butanol both lead to a larger fraction of NRs in bundles as well as to a larger bundle size. We can understand this from the fact that both a higher concentration and butanol increase the free-energy driving force for bundle formation, be it in different ways. The NR concentration has an entropic contribution to the free energy, while butanol increases the enthalpic contribution (i.e., the mutual interaction strength).

Although the size of the NR sheets is not governed by a full thermodynamic equilibrium, it is still clear from the results above that the bundle size is strongly affected by free energy driving for self-assembly. Hence, we still expect an effect of temperature. Importantly, as the temperature changes, not only does the free-energy driving force for assembly change, but kinetic parameters such as the force and frequency of collisions between existing bundles also change, which may allow them to merge or break them apart. Moreover, a higher thermal energy k_BT implies stronger Brownian rotations counteracting magnetic alignment. We investigated the effect of temperature between 20 and 50 °C on the magnetic alignment of long and medium-length NRs.

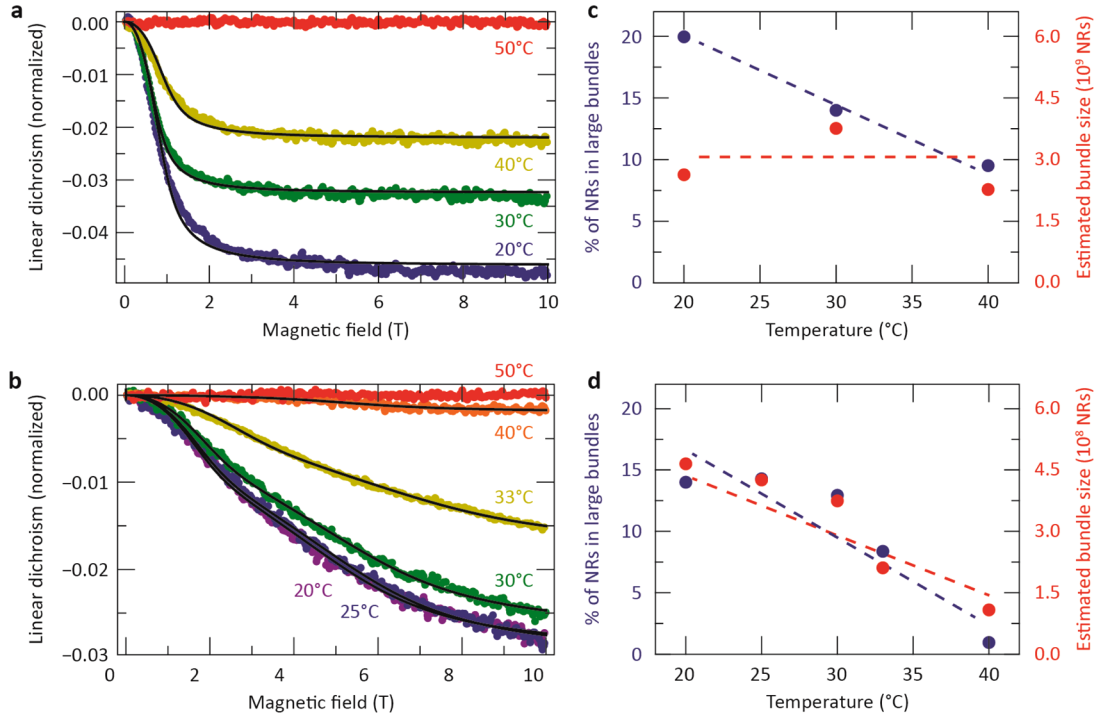

Figure 5. (a,b) Linear dichroism of the sample of (a) long NRs and (b) medium-length NRs as a function of applied magnetic field, for different temperatures. Solid lines are fits to eq 5, where for the medium-length NRs we assumed a bimodal bundle size distribution for a better correspondence. (c,d) Fitted fraction of NRs in bundles (blue) and estimated average bundle size (red) for (c) the long NRs and (d) the medium-length NRs.

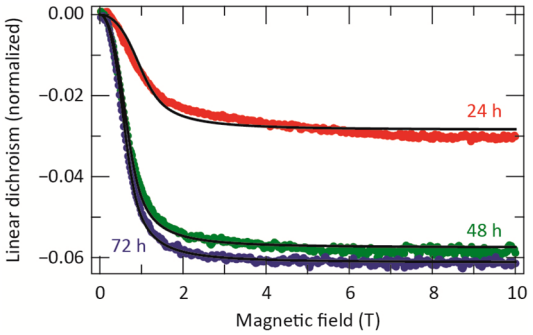

Figure 6. Linear dichroism of the sample of long NRs as a function of applied magnetic field strength for different times after heating to 50 °C and cooling back to room temperature. Restoration of the LD-signal takes place over the time scale of days.

Figure 5 shows the LD-signal up to 10 T of (a) long NRs and (b) medium-length NRs for different temperatures. For both samples there is a clear trend that the magnitude of the LD-signal decreases for increasing temperature. In fact, the LD-signal completely disappears on this temperature range from 20 to 50 °C, corresponding to a mere 10% increase of the thermal energy. Figure 5c,d shows the results of fits to the experimental data: the fraction of NRs in large bundles and the average bundle size. Dashed lines are guides to the eye. As expected, we see trends of decreasing size and number of bundles with increasing temperature.

Finally, we investigate the kinetics of the assembly of NRs into bundles. To this end, we heated the sample of long NRs to above 40 °C until the LD-signal had completely vanished (as in Figure 5). Then, outside the magnet, the sample is allowed to cool down to room temperature. Figure 6 shows how the LD-signal reappears, as the NRs reassemble into bundles. The reassembly occurs over the time scale of days. In fact, after 72 h the LD-signal at saturation reaches a value slightly higher than before the sample went through a heating−cooling cycle (compare to Figures 3 and 4 for the signal of NRs that did not undergo heating−cooling). This long time scale confirms that the self-assembly of NR involves slow growth, merging, and (possibly) breaking of sheets. Hence, we should remark that in our experiments the suspensions have possibly not reached the state of complete equilibrium between the NRs.

CONCLUSIONS

To summarize, using small-angle X-ray scattering (SAXS) and magnetic-field induced linear dichroism (LD) we have investigated large self-assembled bundles in a bulk solution of CdSe/CdS NRs. SAXS proved the existence of ordered NR monolayer structures in the bulk solution with remarkably long inter-NR distances. The magnetic response of individual NRs is so weak that in the LD-measurements we were sensitive only to very large sheets of NRs. Such large bundles can only occur if the NR concentration and NR−NR interactions are sufficiently strong. Indeed, suspensions of short NRs, which experience weak mutual interactions, do not show a LD-signal. We were able to increase the size and number of bundles by increasing the NR concentration or by the addition of nonsolvent. We provide evidence that the settlement of an equilibrium between individual and assembled NR requires days, probably involving growth, merging as well as breaking of existing bundles. Our results shed light on the processes underlying the self-assembly of rod-shaped nanocrystals with relatively strong side-to-side attraction.

METHODS

Chemicals Used. CdO (Sigma-Aldrich, 99%), trioctylphosphine oxide (TOPO, Sigma-Aldrich, 99%), octadecylphosphonic acid (ODPA, Sigma-Aldrich, 97%), trioctylphosphine (TOP, Sigma-Aldrich, 90%), selenium (Aldrich, 98%), and sulfur (Sigma-Aldrich, 99%).

Synthesis of CdSe Nanocrystal Seeds[32]. CdSe nanocrystal seeds were synthesized in 50 mL three-neck flask using a Schlenk-line. A mixture of TOPO (3.0 g), ODPA (0.290 g), and CdO (0.060 g) was kept under vacuum for 2 h at 150 °C. The reaction solution was then heated under nitrogen to 300 °C at a rate of approximately 7 °C/min. The reaction solution became transparent, indicating the formation of Cd-ODPA complexes. Next, 1.5 g of TOP was rapidly injected. After heating to 350−370 °C, the seed formation was initiated by injecting a solution of 0.058 g of Se in 0.360 g of TOP. The reaction was quenched by removing the heating source, and (after cooling to below 100 °C) diluting the mixture with 5 mL of toluene. The final size of the nanocrystals depends on the reaction time, longer reaction times leading to larger seeds. For nanocrystal seeds with 2 nm diameter, the reaction was quenched immediately after the injection of the TOP-Se solution. For larger seeds of 3−4 nm diameter, the reaction solution was kept at high temperature for ∼120 s. The nanocrystal seeds were washed twice by precipitation with methanol and centrifugation. Finally, they were redissolved in toluene and stored inside a glovebox under nitrogen atmosphere.

Synthesis of CdSe/CdS Core/Shell Nanorods[32]. A mixture of CdO (0.09 g), TOPO (3.0 g), and ODPA (0.280g) in a 50 mL three-neck flask was degassed, heated to 150 °C, and kept under vacuum for 2 h. The solution was then heated under nitrogen to 350 °C and 1.5 g of TOP was injected. The reaction solution was kept at 350 °C for 15 min to allow for the temperature to stabilize. TOP-S solution (0.12 g of S in 1.5 g of TOP) and 200 μL of TOP-seeds stock solution (with a NC concentration of 400 μM) were rapidly injected in the flask, upon which the rod-shaped shells form. The NR length was varied by changing the reaction time between 6 and 12 min. The CdSe/CdS dot core/rod shell NRs were washed by precipiation with methanol (10 mL) and centrifugation. The final product was redispersed in toluene (5 mL).

The size of the NRs was determined by transmission electron microscopy (TEM) using a Tecnai microscope operating at 120 kV. The NR concentration was estimated using inductively coupled plasma-atomic emission spectroscopy (ICP-AES), in combination with absorption spectroscopy. Absorption spectra were measured using a PerkinElmer Lambda 950 UV/vis/IR absorption spectrophotometer.

SAXS Measurements. SAXS experiments were performed at the BM-26B DUBBLE beamline of the European Synchrotron Radiation Facility (ESRF) with an incident X-ray energy of 12 keV (1.033 Å) and the Pilatus detector aligned for a q range from 0.02 to 1.5 nm^{-1}, where q is the scattering vector. The NR solution was placed in a round capillary with diameter 0.5 mm and length 80 mm.

Linear Dichroism Measurements. The experiment was performed at the High Magnetic Field Laboratory at the Radboud University Nijmegen. The sample was placed in the temperature-controlled bore of a 33 T Bitter magnet. We used a Xe Lamp as the light source. The transmitted light was guided through a monochromator and a polarizer (set at 45° to the magnetic field direction), followed by a photoelastic modulator (PEM-90, Hinds Instruments, Hillsboro, OR) before passing the sample in a horizontal direction, perpendicular to the magnetic field. The transmitted light was detected by a Si photodiode. Two lock-in amplifiers (SR830, SRS, Sunnyvale, CA) were used to detect the second harmonic of the ac signal, from which the linear dichroism (LD) signal $\Delta A(B)$, can be calculated. CdSe/CdS NRs were dispersed in toluene, and the solution was transferred to a quartz cuvette (thickness 5 mm) (Hellma) for the measurements. The cuvette was carefully sealed with Teflon tape to avoid evaporation of the solvent during the measurement. LD-measurements were carried out with varying the field between 0 and 30 T. The LD-signal $\Delta A(B)$ is normalized to the total absorbance $A(0)$ at zero field, corrected for the absorbance of a reference cuvette containing only toluene: $A(0) = -\log(T(0)/T_{ref})$, where $T(0)$ is the transmission of the sample at zero field and T_{ref} is the transmission of the reference cuvette.

Conflict of Interest: The authors declare no competing financial interest.

Supporting Information Available: Transmission electron microscopy images of the CdSe/CdS NRs, calculation of the magnetic and optical response of self-organized NRs, and investigation of the effect of polydispersity in the bundle size, estimates of the van der Waals interaction, and magnetic-field induced dipolar interaction between NRs. This material is available free of charge *via* the Internet at http://pubs.acs.org.

Acknowledgment. The authors appreciate financial support from the European Union under the Seventh Framework Program (EU-FP7 ITN Herodot). This work is part of the research program of the "Stichting voor Fundamenteel Onderzoek der Materie (FOM)", which is financially supported by the "Nederlandse Organisatie voor Wetenschappelijk Onderzoek (NWO)". We acknowledge the support of HFML-RU/FOM, member of the European Magnetic Field Laboratory (EMFL). Part of this work has been supported by EuroMagNET II under the EU Contract Number 228043. Part of this work was carried out at the European Synchrotron Radiation Facility (ESRF) in Grenoble (France).

REFERENCES AND NOTES

1. Sun, B.; Sirringhaus, H. Solution-Processed Zinc Oxide Field-Effect Transistors Based on Self-Assembly of Colloidal Nanorods. *Nano Lett.* **2005**, *5*, 2408–2413.
2. Hu, J.; Li, L.; Yang, W.; Manna, L.; Wang, L.; Alivisatos, A. P. Linearly Polarized Emission from Colloidal Semiconductor Quantum Rods. *Science* **2001**, *292*, 2060–2063.
3. Rizzo, A.; Nobile, C.; Mazzeo, M.; Giorgi, M.; De Fiore, A.; Carbone, L.; Cingolani, R.; Manna, L.; Gigli, G. Polarized Light Emitting Diode by Long-Range Nanorod Self-Assembling on a Water Surface. *ACS Nano* **2009**, *3*, 1506–1512.
4. Pisanello, F.; Martiradonna, L.; Spinicelli, P.; Fiore, A.; Hermier, J. P.; Manna, L.; Cingolani, R.; Giacobino, E.; De Vittorio, M.; Bramati, A. Dots in Rods as Polarized Single Photon Sources. *Superlattices Microstruct.* **2010**, *47*, 165–169.
5. Huynh, W. U.; Dittmer, J. J.; Alivisatos, A. P. Hybrid Nanorod-Polymer Solar Cells. *Sci.* **2002**, *295*, 2425–2427.
6. Gonzalez-Valls, I.; Lira-Cantu, M. Vertically-Aligned Nanostructures of ZnO for Excitonic Solar Cells: A Review. *Energy Environ. Sci.* **2009**, *2*.
7. Talgorn, E.; Gao, Y.; Aerts, M.; Kunneman, L. T.; Schins, J. M.; Savenjie, T. J.; van Huis, M. A.; van der Zant, S. J.; Houtepen, A. J.; Siebbeles, L. D. A. Unity Quantum Yield of Photogenerated Charges and Band-like Transport in Quantum-Dot Solids. *Nat. Nanotechnol.* **2011**, *6*, 733–739.
8. Tang, J.; Kemp, K. W.; Hoogland, S.; Jeong, K. S.; Liu, H.; Levina, L.; Furukawa, M.; Wang, X.; Debnath, R.; Cha, D.; *et al.* Colloidal-Quantum-Dot Photovoltaics Using Atomic-Ligand Passivation. *Nat. Mater.* **2011**, *10*, 765–771.
9. Vanmaekelbergh, D. Self-Assembly of Colloidal Nanocrystals as Route to Novel Classes of Nanostructured Materials. *Nano Today* **2011**, *6*, 419–437.
10. Shevchenko, E. V.; Talapin, D. V.; Kotov, N. A.; O'Brien, S.; Murray, C. B. Structural Diversity in Binary Nanoparticle Superlattices. *Nature* **2006**, *439*, 55–59.
11. Shevchenko, E. V.; Kortright, J.; Talapin, D. V.; Aloni, S.; Alivisatos, A. P. Quasi-Ternary Nanoparticle Superlattices Through Nanoparticle Design. *Adv. Mater.* **2007**, *19*, 4183–4188.
12. Talapin, D. V.; Shevchenko, E. V.; Bodnarchuk, M. I.; Ye, X.; Chen, J.; Murray, C. B. Quasicrystalline Order in Self-Assembled Binary Nanoparticle Superlattices. *Nature* **2009**, *461*, 964–967.
13. Evers, W. H.; Nijs, B.; De Filion, L.; Castillo, S.; Dijkstra, M.; Vanmaekelbergh, D. Entropy-Driven Formation of Binary Semiconductor-Nanocrystal Superlattices. *Nano Lett.* **2010**, *10*, 4235–4241.
14. Dong, A.; Chen, J.; Vora, P. M.; Kikkawa, J. M.; Murray, C. B. Binary Nanocrystal Superlattice Membranes Self-Assembled at the Liquid-Air Interface. *Nature* **2010**, *466*, 474–477.
15. Evers, W. H.; Goris, B.; Bals, S.; Casavola, M.; de Graaf, J.; van Roij, R.; Dijkstra, M.; Vanmaekelbergh, D. Low-Dimensional Semiconductor Superlattices Formed by Geometric Control over Nanocrystal Attachment. *Nano Lett.* **2013**, *13*, 2317–2323.
16. Pietra, F.; Rabouw, F. T.; Evers, W. H.; Byelov, D. V.; Petukhov, A. V.; de Mello Donegá, C.; Vanmaekelbergh, D. Semiconductor Nanorod Self-Assembly at the Liquid/Air Interface Studied by *in Situ* GISAXS and *ex Situ* TEM. *Nano Lett.* **2012**, *12*, 5515–5523.
17. Van der Stam, W.; Gantapara, A. P.; Akkerman, Q. A.; Soligno, G.; Meeldijk, J. D.; van Roij, R.; Dijkstra, M.; de Mello Donega, C. Self-Assembly of Colloidal Hexagonal Bipyramid- and Bifrustum-Shaped ZnS Nanocrystals into Two-Dimensional Superstructures. *Nano Lett.* **2014**, *14*, 1032–1037.
18. Rabouw, F. T.; Lunnemann, P.; van Dijk-Moes, R. J. A.; Frimmer, M.; Pietra, F.; Koenderink, A. F.; Vanmaekelbergh, D. Reduced Auger Recombination in Single CdSe/CdS Nanorods by One-Dimensional Electron Delocalization. *Nano Lett.* **2013**, *13*, 4884–4892.
19. Granados del Águila, A.; Jha, B.; Pietra, F.; Groeneveld, E.; de Mello Donegá, C.; Maan, J. C.; Vanmaekelbergh, D.; Christianen, P. C. M. Observation of the Full Exciton and Phonon Fine Structure in CdSe/CdS Dot-in-Rod Heteronanocrystals. *ACS Nano* **2014**, *8*, 3921–5931.
20. Zanella, M.; Gomes, R.; Povia, M.; Giannini, C.; Zhang, Y.; Riskin, A.; Van Bael, M.; Hens, Z.; Manna, L. Self-Assembled Multilayers of Vertically Aligned Semiconductor Nanorods on Device-Scale Areas. *Adv. Mater.* **2011**, *23*, 2205–2209.
21. Singh, A.; Gunning, R. D.; Ahmed, S.; Barrett, C. A.; English, N. J.; Garate, J.-A.; Ryan, K. M. Controlled Semiconductor Nanorod Assembly from Solution: Influence of Concentration, Charge and Solvent Nature. *J. Mater. Chem.* **2012**, *22*, 1562.
22. Hung, A. M.; Oh, T.; Cha, J. N. Facile Thermal Treatment Process for Assembling Vertically Aligned Semiconductor Nanorods in Solution. *Nanoscale* **2012**, *4*.
23. Mattoussi, H.; Cumming, A. W.; Murray, C. B.; Bawendi, M. G.; Ober, R. Characterization of CdSe Nanocrystallite Dispersions by Small Angle X-Ray Scattering. *J. Chem. Phys.* **1996**, *105*, 9890.
24. Van Rijssel, J.; Erne, B. H.; Meeldijk, J. D.; Casavola, M.; Vanmaekelbergh, D.; Meijerink, A.; Philipse, A. P. Enthalpy

and Entropy of Nanoparticle Association from Temperature-Dependent Cryo-TEM. *Phys. Chem. Chem. Phys.* **2011**, *13*, 12770–12774.
25. Widmer-Cooper, A.; Geissler, P. Orientational Ordering of Passivating Ligands on CdS Nanorods in Solution Generates Strong Rod-Rod Interactions. *Nano Lett.* **2014**, *14*, 57–65.
26. Löwik, D. W. P. M.; Shklyarevskiy, I. O.; Ruizendaal, L.; Christianen, P. C. M.; Maan, J. C.; van Hest, J. C. M. A Highly Ordered Material from Magnetically Aligned Peptide Amphiphile Nanofiber Assemblies. *Adv. Mater.* **2007**, *19*, 1191–1195.
27. Gielen, J. C.; Shklyarevskiy, I. O.; Schenning, A. P. H. J.; Christianen, P. C. M.; Maan, J. C. Using Magnetic Birefringence to Determine the Molecular Arrangement of Supramolecular Nanostructures. *Sci. Technol. Adv. Mater.* **2009**, *10*, 14601.
28. Gielen, J. C.; Wolffs, M.; Portale, G.; Bras, W.; Henze, O.; Kilbinger, A. F. M.; Feast, W. J.; Maan, J. C.; Schenning, A. P. H. J.; Christianen, P. C. M. Molecular Organization of Cylindrical Sexithiophene Aggregates Measured by X-Ray Scattering and Magnetic Alignment. *Langmuir* **2009**, *25*, 1272–1276.
29. Micali, N.; Engelkamp, H.; van Rhee, P. G.; Christianen, P. C. M.; Monsù Scolaro, L.; Maan, J. C. Selection of Supramolecular Chirality by Application of Rotational and Magnetic Forces. *Nat. Chem.* **2012**, *4*, 201–207.
30. Liebi, M.; van Rhee, P. G.; Christianen, P. C. M.; Kohlbrecher, J.; Fischer, P.; Walde, P.; Windhab, E. J. Alignment of Bicelles Studied with High-Field Magnetic Birefringence and Small-Angle Neutron Scattering Measurements. *Langmuir* **2013**, *29*, 3467–3473.
31. Van Rhee, P. G.; Zijlstra, P.; Verhagen, T. G. A.; Aarts, J.; Katsnelson, M. I.; Maan, J. C.; Orrit, M.; Christianen, P. C. M. Giant Magnetic Susceptibility of Gold Nanorods Detected by Magnetic Alignment. *Phys. Rev. Lett.* **2013**, *111*, 127202.
32. Carbone, L.; Nobile, C.; De Giorgi, M.; della Sala, F.; Morello, G.; Pompa, P.; Hytch, M.; Snoeck, E.; Fiore, A.; Franchini, I. R.; *et al.* Synthesis and Micrometer-Scale Assembly of Colloidal CdSe/CdS Nanorods Prepared by a Seeded Growth Approach. *Nano Lett.* **2007**, *7*, 2942–2950.
33. Bertoni, G.; Grillo, V.; Brescia, R.; Ke, X.; Bals, S.; Catellani, A.; Li, H.; Manna, L. Direct Determination of Polarity, Faceting, and Core Location in Colloidal Core/Shell Wurtzite Semiconductor Nanocrystals. *ACS Nano* **2012**, *6*, 6453–6461.
34. Pedersen, J. S. Analysis of Small-Angle Scattering Data from Colloids and Polymer Solutions: Modeling and Least-Squares Fitting. *Adv. Colloid Interface Sci.* **1997**, *70*, 171–210.
35. Guinier, A. *X-Ray Diffraction in Crystal, Imperfect Crystals, and Amorphous Bodies*; Dover: New York, 1994.
36. Kemp, J. C.; Henson, G. D.; Steiner, C. T.; Powell, E. R. The Optical Polarization of the Sun Measured at a Sensitivity of Parts in Ten Million. *Nature* **1987**, *326*, 270–273.
37. Kamal, J. S.; Gomes, R.; Hens, Z.; Karvar, M.; Neyts, K.; Compernolle, S.; Vanhaecke, F. Direct Determination of Absorption Anisotropy in Colloidal Quantum Rods. *Phys. Rev. B* **2012**, *85*, 35126.
38. Broersma, S. The Magnetic Susceptibility of Organic Compounds. *J. Chem. Phys.* **1949**, *17*, 873.
39. Israelachvili, J. *Intermolecular and Surface Forces*; Academic Press: London, 1985.
40. Crespo, P.; Litrán, R.; Rojas, T. C.; Multigner, M.; de la Fuente, J. M.; Sánchez-López, J. C.; García, M. A.; Hernanod, A.; Penadés, S.; Fernández, A. Permanent Magnetism, Magnetic Anisotropy, and Hysteresis of Thiol-Capped Gold Nanoparticles. *Phys. Rev. Lett.* **2004**, *93*, 087204.
41. Kortschot, R. J.; Van Rijssel, J.; Van Dijk-Moes, R. J. A.; Erné, B. H. Equilibrium Structures of PbSe and CdSe Colloidal Quantum Dots Detected by Dielectric Spectroscopy. *J. Phys. Chem. C* **2014**, *118*, 7185–7194.
42. Bates, M. A.; Frenkel, D. Nematic–Isotropic Transition in Polydisperse Systems of Infinitely Thin Hard Platelets. *J. Chem. Phys.* **1999**, *110*, 6553–6559.